Unclassified

SECURITY CLASSIFICATION OF THIS PAGE

(2)

REPORT DOCUMENTATION PAGE

Form Approved
OMB No 0704 0188
Exp Date Jun 30 1986

1a REPORT SECURITY CLASSIFICATION: Unclassified	1b RESTRICTIVE MARKINGS: DTIC FILE COPY
	3 DISTRIBUTION/AVAILABILITY OF REPORT: Approved for public release; distribution unlimited
AD-A205 076	5 MONITORING ORGANIZATION REPORT NUMBER(S): R&D 4697-MS-01

DTIC ELECTED SCHEDULE FEB 1 6 1989 D Cs

6a NAME OF PERFORMING ORGANIZATION: The Hebrew University of Jerusalem	6b OFFICE SYMBOL (If applicable):
6c ADDRESS (City, State, and ZIP Code): Department of Inorganic and Analytical Chemistry, Jerusalem 91904 Israel	7b ADDRESS (City, State, and ZIP Code): Box 65 FPO NY 09510-1500
7a NAME OF MONITORING ORGANIZATION: USARDSG-UK European Research Office	
8a NAME OF FUNDING/SPONSORING ORGANIZATION: European Research Office USARDSG-UK ARO-E	8b OFFICE SYMBOL (If applicable):
8c ADDRESS (City, State, and ZIP Code): Box 65 FPO NY 09510-1500	9 PROCUREMENT INSTRUMENT IDENTIFICATION NUMBER: DAJA45-85-C-0051

10 SOURCE OF FUNDING NUMBERS

PROGRAM ELEMENT NO.	PROJECT NO	TASK NO	WORK UNIT ACCESSION NO
61102A	1L161102BH57	0	

11 TITLE (Include Security Classification)
(U) Transparent Glass Ceramics Doped by Chromium(III) and Chromium(III) and Neodymium(III) as New Materials for Lasers and Luminescent Solar Concentrators

12 PERSONAL AUTHOR(S)
Professor Renata Reisfeld

13a TYPE OF REPORT	13b TIME COVERED	14 DATE OF REPORT (Year, Month, Day)	15 PAGE COUNT
Final	FROM 1.10.85 TO 30.6.88	1988 December 27	34

16 SUPPLEMENTARY NOTATION

17 COSATI CODES		
FIELD	GROUP	SUB-GROUP
M102		
2006		

18 SUBJECT TERMS (Continue on reverse if necessary and identify by block number)
glass ceramics, chromium, tunable lasers, PASM

19 ABSTRACT (Continue on reverse if necessary and identify by block number)

Transparent glass ceramics doped by chromium(III) and codoped by chromium(III) and neodymium(III) having the structure of spinel, gahnite, petalite and mullite were prepared.
Steady state spectroscopy (absorption and emission) as well as time resolved spectroscopy were studied at room temperature and varying temperatures down to that of liquid helium.
Quantum efficiency of chromium(III) at room temperature is high, between 0.9 and 1.0, in mullite glass ceramics. Cross section for laser and laser threshold were calculated.
The potential application of these materials for tunable lasers in the red and near infrared is described.

20 DISTRIBUTION/AVAILABILITY OF ABSTRACT	21 ABSTRACT SECURITY CLASSIFICATION
☒ UNCLASSIFIED/UNLIMITED ☒ SAME AS RPT ☒ DTIC USERS	Unclassified

22a NAME OF RESPONSIBLE INDIVIDUAL	22b TELEPHONE (Include Area Code)	22c OFFICE SYMBOL
Dr. Wilbur C. Simmons	01-409 4423	AMXSN-UK-RM

DD FORM 1473, 84 MAR — 83 APR edition may be used until exhausted. All other editions are obsolete.

SECURITY CLASSIFICATION OF THIS PAGE
Unclassfied

(1)

TRANSPARENT GLASS CERAMICS DOPED BY CHROMIUM(III) AND CHROMIUM(III) AND NEODYMIUM(III) AS NEW MATERIALS FOR LASERS AND LUMINESCENT SOLAR CONCENTRATORS

Research supported by U.S. Army
under contract No. DAJA 45-85-C-0051

Final Report

1.10.85 - 30.6.88

Submitted by

Professor Renata Reisfeld
Department of Inorganic and Analytical Chemistry
The Hebrew University of Jerusalem
Jerusalem 91904 Israel

to

European Office of the U.S. Army
223/231 Old Marylebone Rd.
London WC1 5TH
England

and

Army Materials and Mechanics
Research Center, Watertown,
Massachusetts 02172
U.S.A.

This work was performed together with Alla Buch, Mehdi Bouderbala, Georges Boulon, Marek Eyal, Esther Greenberg, Moshe Ish-Shalom, Yehoshua Kalisky, Anna Kisilev, Anne-Marie Lejus and Vincent Poncon.

I am most grateful to Professor C.K. Jørgensen of the University of Geneva for fruitful discussions.

CONTENTS

ABSTRACT

This is the final report on "Transparent glass ceramics doped by chromium(III) and chromium(III) and neodymium(III) as new materials for lasers and luminescent solar concentrators", of our 3 year project performed for the European Office of the US Army and the Army Materials and Mechanics Research Center.

The purpose of the study was to prepare and optically study glass-ceramics doped by Cr(III) and their potential application for tunable lasers.

The work is completed now and has been published in several papers under the Army contract:

1. R. Reisfeld, A. Kisilev, A. Buch and M. Ish-Shalom. Spectroscopy and EPR of chromium(III) in mullite transparent glass-ceramics. Chem. Phys. Lett., 129 (1986) 446.
2. R. Reisfeld, A. Kisilev, A. Buch and M. Ish-Shalom. Transparent glass-ceramics doped by chromium(III): Spectroscopic properties and characterization of crystalline phases. J. Non-Cryst. Solids, 91 (1987) 333.
3. Y. Kalisky, V. Poncon, G. Boulon, R. Reisfeld, A. Buch and M. Ish-Shalom. Time-resolved spectroscopy of chromium(III) in mullite transparent glass-ceramics. Chem. Phys. Lett., 136 (1987) 368.
4. R. Reisfeld and C.K. Jørgensen. Excited states of chromium(III) in translucent glass-ceramics as prospective laser materials. Structure and Bonding, 69 (1988) 63.
5. R. Reisfeld, M. Eyal, A. Buch and M. Ish-Shalom. Energy transfer from chromium(III) to neodymium(III) in mullite glass-ceramics. Chem. Phys. Lett., 147 (1988) 148.

The above publications and the following previous publications are attached to this report:

1. R. Reisfeld. Potential uses of chromium(III)-doped transparent glass ceramics in tunable lasers and luminescent solar concentrators. Materials Science and Engineering, 71 (1985) 375.
2. A. Buch, M. Ish-Shalom, R. Reisfeld, A. Kisilev and E. Greenberg. Transparent glass ceramics: preparation, characterization and properties. Materials Science and Engineering, 71 (1985) 383
3. M. Bouderbala, G. Boulon, R. Reisfeld, A. Buch, M. Ish-Shalom and A-M. Lejus. Time-resolved and temperature-dependent spectra of chromium(III) in glasses and spinel-type glass-ceramics. Chem. Phys. Lett., 121 (1985) 535.

The report also includes the theoretical consideration of the spectroscopy of chromium(III) and the calculation of laser cross-section of chromium(II) in mullite glass-ceramics and its threshold for lasing. Formulae are provided which enable calculation of similar data in other glass-ceramics.

1. INTRODUCTION

Cr(III) ion in inorganic glasses has been considered as a material for luminescent solar concentrators (LSC) as it absorbs in the major part of the solar spectrum and emits in the near IR where the sensitivity of the silicon photovoltaic cell is at its maximum [1,2]. However its notoriously low quantum efficiency in glasses [3,4] brought us to look for a material which is as transparent and mechanically workable as glass and which has a much higher quantum efficiency of Cr(III), similar to that of crystals [5,6].

The research has resulted in a many publications dealing with spectroscopic and related properties of Cr(III) in transparent glass-ceramics [7-23]. In these materials Cr(III) is concentrated in submicroscopic crystallites having dimensions smaller than the wavelength of visible radiation. Line-narrowing experiments have been performed on Cr(III) in some of the glasses and glass-ceramics [22,23]. These enable the establishment of the local site symmetry of Cr(III) in the ceramics. Information of this type can be derived from the size of R_1 - R_2 separation, the ratio of the oscillator strengths and the polarization of the R lines.

2. SPECTROSCOPY OF CHROMIUM(III)

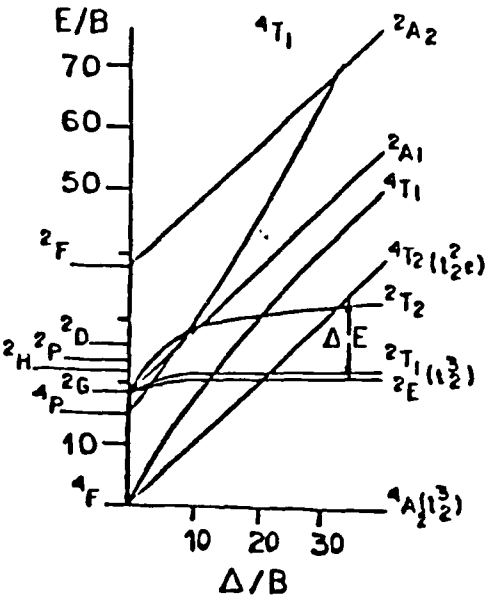

Figure 1. Energy levels as a function of the ligand field strength in units of the Racah-parameter B for octahedrally coordinated d^3 systems such as Cr(III).

The spectroscopy of Cr(III) in glass-ceramics and the analogy with transition elements spectroscopy as developed by modern theories has been discussed in great detail recently [24]. The absorption and luminescence of Cr(III) originates from transitions in the unfilled 3d electronic shell. Such transitions are Laporte-forbidden in sites having a centre of symmetry [25,26]. The designations of the transitions in Cr(III) in octahedral symmetry have been elaborated in the classic work of Sugano et al. [27] and its relevance to LSCs has been discussed recently [1]. Figure 1 shows the ligand field of the Cr(III) energy levels in an octahedral coordination: on the left-hand side are the Russell-Saunders terms of free Cr(III), and on the right-hand side the group theoretical designations for the symmetry sites in octahedral symmetry [25,26]. The horizontal variable Δ/B, the ratio of the sub-shell energy difference Δ (= 10 Dq) to the Racah parameter B (separating Russell-Saunders terms such as 15 B between ^4P and ^4F of the d^3 (or the d^7) configuration). In this diagram, both the ground state $^4A_2$ and the excited state ^2E arise from the lower set (in octahedral symmetry) of d orbitals $(t_2)^3$ whereas $^4T_2$ belongs to $(t_2)^2(e)^1$.

In the spin forbidden transition $^2E \dashrightarrow {}^4A_2$ there is no change in the geometry of the electronic orbitals and the equilibrium position of the ground and excited configuration is almost unchanged (see Fig.2); the transition is sharp, the vibronic interaction weak and the situation of the R lines in ruby or alexandrite resembles that of rare earths. In contrast, the spin-allowed transition $^4T_2 \dashrightarrow {}^4A_2$ arises from the e set to the t_2 set. Since the two e orbitals are pointed along the axes of the octahedron in the direction of the ligands, they participate in anti-bonding molecular orbitals, and the presence of one electron in these orbitals in the excited state causes a distortion and an increase in equilibrium internuclear distance between Cr(III) and the ligands. The extension of the electronic function results in its much stronger interaction with the vibrational modes. The situation is evident from the configurational diagram (see Fig.2) and as described here is characteristic of the general behaviour of molecules and ions which exhibit strong vibronic coupling

when the transitions are spin-allowed, and a weak coupling when the transitions are spin-forbidden. Apparently the vibronic coupling of Cr(III) in an amorphous material where no symmetry restrictions occur is much stronger than in a crystal of similar chemical composition.

Whether the energy of $^4T_2$ is higher than the energy of ^2E or vice versa in a given chromium compound depends on the strength of the ligand field acting on Cr(III). This can be seen directly from Fig.2

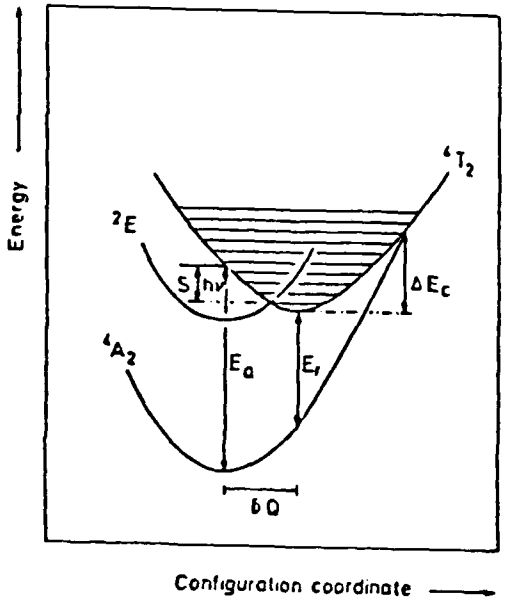

Figure 2. Congfiguration coordinate diagram for the ground state $^4A_2$ and the excited $^4T_2$ and ^2E states for Cr(III) in intermediate fields.

where E represents the energy difference between the $^4T_2$ and ^2E states [6]. Experimentally it is measured from the position of the zero-phonon $^4T_2$ and ^2E bands. The values of both energies are equal and $\Delta E = 0$ for $\Delta/B = 20$ (intermediate field); high fields have Δ/B greater than 20 and $^4T_2$ above the ^2E level. Besides the variation in with interatomic distance, the other atoms bound to the nearest-neighbour oxygen atoms may have some influence.

Glasses provide low field Cr(III) sites in which the zero-phonon $^4T_2$ level lies below the zero-phonon ^2E state. In these low field cases the room temperature Cr(III) emission from $^4T_2$ consists of a broad unstructured band centred in the near IR. From electrostatic considerations a more open structure arises from the larger distance between Cr(III) and its ligands and results in low fields. Quantum yields for luminescence are low in glass hosts; for example the

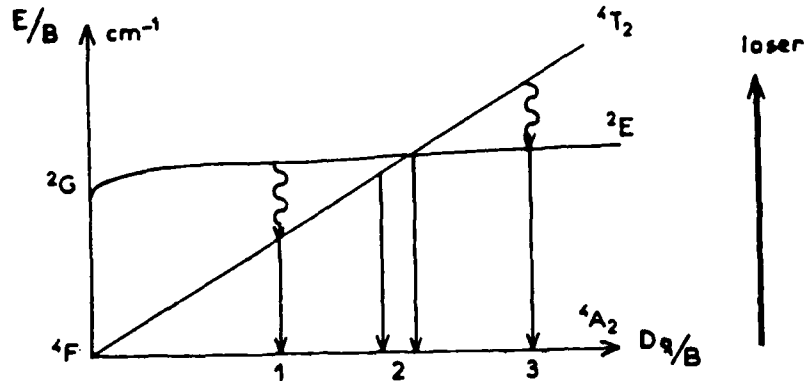

Simplified Tanabe-Sugano diagram of the Cr(III) ion. We show here only the two first excited states occurring in the fluorescence mechanism.

1. low crystal field
2. intermediate crystal
3. high crystal field

The laser pumps one vibrational level $^4T_2$ excited state and the arrows indicate the nonradiative relaxation between $^4T_2$ and ^2E levels.

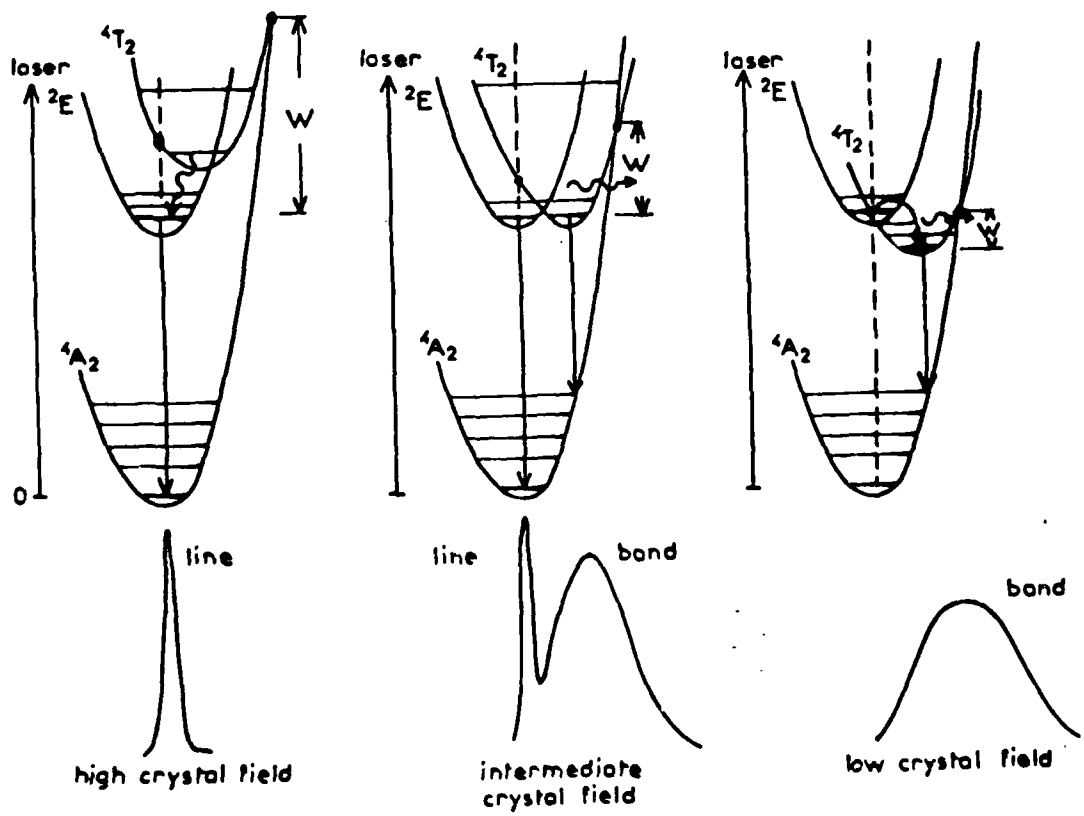

Configuration coordinate diagrams of the Cr(III) levels in the three cases shown schematically in the upper figure.

highest quantum yield of Cr(III) found to date in silicate glass is 11%-17%. As already mentioned above the best efficiencies of 22% for $^4T_2$ --> $^4A_2$ are obtained for lithium lanthanum phosphate (LLP) glasses [2,28]. Quite recently germanate glasses doped by Cr(III) have revealed a quantum efficiency of 25% [29].

3. RECENT PROGRESS IN THEORY

The absorption spectra of compounds containing a partly filled 3d, 4d or 5d shell were to a large extent [26,27,30-32] rationalized by "ligand field" theory applied to aqua ions $M(OH_2)_6^{+z}$, ammonia complexes $M(NH_3)_n(OH_2)_{6-n}^{+z}$, complexes of multidentate (synthetic or biological) aminopolycarboxylate anions such as ethylenediaminetetraacetate $M(edta)(OH_2)_x^{+z-4}$ and glycinate $M(NH_2CO_2)_n(OH_2)_{6-2n}^{+z-n}$ in solution, for which a rich material of formation constants were available, even before 1960. Related to the operation in 1960 of the first laser [ruby $Cr_xAl_{2-x}O_3$] much work was initiated on absorption and luminescence spectra of d-group ions incorporated at low concentration in colourless crystals of known structure [33-35]. The bright colours of many minerals may be ascribed to the simultaneous presence of iron(II) and iron(III) in (otherwise colourless) silicate minerals, producing strong electron transfer bands [26]. Analogous to Prussian Blue, $AFe^{II}(CN)_6Fe^{III}$ such colours can also be intensely blue, like in sapphire $Fe_x^{II}Ti_x^{IV}Al_{2-2x}O_3$ through simultaneous presence of Ti(III) and Ti(IV) usually provide brown-purplish colours of glass-ceramics [8] and of Al_2O_3 [36]. Glasses are in a similar situation as solutions from a spectroscopic viewpoint. EXAFS can provide valuable information about the distances (with precision around 1%) from a given element (even at moderate concentration) to neighbour nuclei of other elements. Optical spectra of group 3d ions in glasses have brought relatively undramatic conclusions about the local symmetry. Both Cr(III) and Ni(II) in oxide and fluoride glasses [37] remain close to regular octahedral. The major variation, like in crystalline mixed oxides [26,35,38] seems to be the one-electron energy difference [between the two anti-bonding d-orbitals having angular functions proportional to (x^2-y^2) and to $(3z^2-r^2)$, and the

three roughly non-bonding orbitals (xy), (xz) or (zy)] decreasing some 5% [24] for each percent increase of the chromium-oxygen internuclear distance R. The rationalization for octahedral symmetry is that d^3 systems such as Cr(III) have no anti-bonding electron, compared to the average value 4 q/10 = 1.2 electron in a d^4 system with spherically symmetric groundstate [like Mn(II) and Fe(III) for q = 5 and S = 5/2]. Also d^8 systems such as octahedral Ni(II) have two anti-bonding electrons rather than the average value 3.2, again avoiding 1.2 anti-bonding electron. This situation is entirely different in the 4f group, where the "ligand field" effects are 10 to 50 times weaker [39] than in the d-groups, and where the preference for a given coordination number N and a specific stereochemistry is far less pronounced, both in glasses [40] and in crystals [41,42].

3.1 Intermediate Coupling in the 11 Kramers Doublets Formed by $^4T_2$, ^2E and $^2T_1$

The ruby $Cr_xAl_{2-x}O_3$ (for small x) is an almost ideal material for detecting the doublets, ^2E(14418 and 14447 cm^{-1}) and $^2T_1$ at slightly higher energy, well below the first broad, stronger transition to $^4T_2$ (having the maximum at 18100 cm^{-1}), and the last sharp transition to $^2T_2$ at 21000 cm^{-1} situated between the latter quartet, and the next one ($^4T_1$) at 24400 cm^{-1}. In solution, ^2E can be observed [43] as a sharp, weak band at 14350 cm^{-1} (667 nm) in the oxalate complex $Cr(O_2C_2O_2)_3^{-3}$ and in the aqua ion as a shoulder at 14950 cm^{-1} (669 nm). Around 1960, it was felt that the spin-forbidden transition to ^2E would become very difficult to find, when closer to $^4T_2$ (not so much because it is weak in an absolute sense, but because it broadens and at the same time is superposed by the far stronger $^4T_2$ band). Nevertheless, the urea complex $Cr(OC(NH_2)_2)_6^{+3}$ shows a highly complicated contour of the transition to $^4T_2$ [44,45] and the most clear-cut example in crystals is the cubic elpasolite-type K_2NaCrF_6 where two minor, sharp peaks indicate ^2E and $^2T_1$ at lower wave-numbers than 16200 cm^{-1} of the maximum of $^4T_2$, and a shoulder at $^2T_2$ at 22000 cm^{-1} [46]. However, it is also clear that Cr(III) in such cases behaves rather similarly to Ni(II) showing crossing of ^1E with $^3T_1$ at

lower, and with $^3T_2$ at higher Δ values [47,48]. Griffith [49] pointed out that in such situations, the double-group quantum numbers Γ_J replace the characterization of energy levels by the (upper left superscript) multiplicity (2S + 1) and the symmetry types (such as A_1,A_2, E, T_1 and T_2 in the point group O_h) exactly like monatomic entities conserve J when deviations from Russell-Saunders coupling no longer allow defined S and L values [50].

In gaseous Cr(III) the Lande parameter ζ_{3d} is close to 270 cm^{-1} as can be seen from the width 956 cm^{-1} of the lowest term ^4F (having the first-order width [50] (3 + 1/2) ζ_{nl}). This Lande parameter is nearly twice the ζ_{2p} = 150 cm^{-1} in the oxygen atom, and almost half as large as ζ_{3d} = 630 cm^{-1} in gaseous Ni(II). However, this is still much less than ζ_{5d} in $5d^3$ rhenium(IV) hexahalide complexes [51] and the isoelectronic gaseous molecule IrF_6 all quite close to 3000 cm^{-1}. These 5d group examples show that chemical bonding decreases the effects of spin-orbit coupling relative to the gaseous ion, much in the same way as the nephelauxetic effect [26,52] is the decrease of the S.C.S.(Slater-Condon-Shortley) parameters of inter-electronic repulsion [50], the values for gaseous Cr(III) being multiplied by a factor between 0.9 for the least covalent fluorides [37] to 0.4 for the most covalent Cr(III) compounds. Frequently, the increase of S.C.S. parameters with ionic charge is cancelled by the more extensive covalent bonding in the higher (isoelectronic) oxidation state, as known from many instances of Cr(III) and Mn(IV) in similar environments [26] or the $3d^5$ Mn(II) and Fe(III). On the whole, the major effect of deviations from Russell-Saunders coupling in octahedral d-group complexes is intensification of spin-forbidden transitions, as seen in $4d^6$ rhodium(III) and somewhat stronger absorption bands [31,53] in $5d^6$ iridium(III) which can be compared with the determinants of intermediate coupling in O_h [54].

4. TYPES OF GLASS-CERAMICS STUDIED

The glass-ceramics studied were spinel-type [8,11,15], gahnite-type [8,12,14,17], a petalite-like phase [2,7], β-quartz [7,16], mullite [13,16,18,22], virgilite [17] and borates [23]. The

corresponding minerals have the crystal type and (frequently rather idealized) chemical composition:

spinel: cubic $MgAl_2O_4$

gahnite (spinel-type): $ZnAl_2O_4$

petalite: monoclinic $LiAlSi_4O_{10}$

virgilite: hexagonal $Li_xAl_xSi_{3-x}O_6$

mullite: orthorhombic $Al_6Si_2O_{13}$

corderite: orthorhombic $Mg_2Al_4Si_5O_{18}$

X-ray diffraction studies of glass-ceramics reveal similarities with the synthetic crystals [12,14,15].

Glass-ceramics obtained at various experimental conditions of nucleation and thermal treatment consist of a crystalline phase and a residual glassy phase. A detailed spectroscopic study of the steady state fluorescence, absorption, decay dynamics (by means of selective laser spectroscopy) as well as electron paramagnetic resonance reveals the detailed nature of the crystalline phases.

The crystalline phases of the glass-ceramics, as compared with synthetic "real" crystals [12,15,17,18,55] of similar composition to the crystals, are prepared by firing and annealing a mixture of stoichiometric amounts of the corresponding oxides. The materials are characterized by steady state and time-resolved spectroscopy, X-rays and EPR spectroscopy. An analogy was found in the spectroscopic properties and high efficiency of fluorescence between Cr(III)in glass-ceramics and crystals [16].

Nucleation is obtained by use of refractory oxides, such as titanium oxide, zirconium oxide [16] and iron(III) oxide [56]. Cr(III) can also serve as a nucleating agent as shown by Small Angle Neutron Scattering (SANS) and Small Angle X-ray Scattering (SAXS) in the case of cordierite glass, of the starting composition, 52 SiO_2, 34.7 Al_2O_3, 12.5 MgO and 0.8 Cr_2O_3 [57], and also for formation of spinel-type glass-ceramics. These techniques give information about particle size. The nucleation of spinel occurs after diffusion of Cr(III) through the bulk of the glass. Heating of the glass at 850°C for 2 hours results in spinel with particle size of 40 Å dispersed in the glassy phase.

The particle size increases after additional heat treatment and may be as high as 280 Å [58].

5. STEADY STATE SPECTROSCOPY

Steady state absorption allows determination of the ligand field strength acting on the Cr(III) ion. The absorption due to $^4A_2$--> $^4T_2$ spin-allowed transition peaks around 650 to 560 nm [16]. As a result of stronger ligand field which is exerted on Cr(III) having shorter distances to its ligating oxygens in more rigid glass-ceramics than glasses the $^4A_2$--> $^4T_2$ absorption peak is shifted to shorter wavelengths, i.e. higher energies.

Table I. Ligand field parameter Δ (in the unit 1000 cm^{-1}) for $Cr(III)O_6$ in glass-ceramics (g.c.); Solids and complexes in solution.

Spinel-type g.c.	original glass	15.5	
"	glassy micro-phase	15.95	
"	micro-crystallites	17.25	
β-quartz g.c.	glassy micro-phase	16.0	
"	micro-crystallites	16.8	
Petalite-like g.c.	original glass	15.6	
"	glassy micro-phase	16.0	
"	micro-crystallites	17.5	
Various silicate glasses			15.2-15.5
Lithium-lanthanum phosphate glass			15.45
Alexandrite $Al_{2-x}Cr_xBeO_4$			17.35
Spinel $MgAl_{2-x}Cr_xO_4$			18.2
Spinel-type $MgAlCrO_4$			17.65
Ruby $Al_{2-x}Cr_xO_3 (x < 0.04)$			18.0
Greyish-pink $Al_{1.6}Cr_{0.4}O_3$			17.55
$Cr(C_2O_4)_3^{-3}$ [oxalate complex]			17.5
$Cr(OH_2)_6^{+3}$ in water			17.45

Table I presents ligand field parameters obtained from the absorption peaks of the $^4A_2 \rightarrow {}^4T_2$ transition of Cr(III) in glasses and glass-ceramics.

Comparison of the value in Table I shows that the ligand field of Cr(III) in the crystalline phase of the glass ceramics is higher than in the glassy phases or in the glasses and its value is comparable to that of Cr(III) in ruby (and alexandrite). The ^2E level is 1000-3000 cm^{-1} below the minimum of the $^4T_2$ level. Such a situation permits thermal equilibration between the two levels as has been found previously in many complexes and crystals.

6. STEADY STATE EMISSION

The emission of Cr(III) in glass-ceramics differs in shape and quantum efficiency from that of glasses. It is usually composed of a broad emission peaking around 750-900 nm arising from the $^4T_2 \rightarrow {}^4A_2$ spin-allowed transition which is usually excited at the absorption around 625 nm, and a sharp well-resolved emission around 680-700 nm due to $^2E \rightarrow {}^4A_2$ transitions from octahedrally distorted single Cr(III) sites and pairs. Figure 3 presents an example [11,15] of emission spectra measured at room temperature and at 4K for a spinel-type glass-ceramics, (Ac), synthetic spinel crystal $MgAl_2O_4$ and mixed crystal of $Mg_{1.2}Ti_{0.2}Al_{1.6}O_4$.

The emission spectrum is composed of the $^2E \rightarrow {}^4A_2$ emission which is characteristic for Cr(III) in the crystals with a large field strength, and of the wide $^4T_2 \rightarrow {}^4A_2$ emission in the glass and low field crystalline sites. The $^2E \rightarrow {}^4A2$ emission reveals a complex structure which is well resolved at 4K [11]. In order to understand the origin of various bands we need to know the crystalline structure of spinels and sites into which Cr(III) can enter.

The usual "normal spinel" is $A^{(4)}B_2{}^{(6)}X_4$ where A is a divalent cation, B is a trivalent cation and X a divalent anion. The symbol (4) designates tetrahedral coordination and (6) octahedral coordination. However spinels are known to undergo inversion, the formula of "inverse spinel" being $B^{(4)}[AB]^{(6)}X_4$. The degree of the inversion

depends on the conditions of crystallization. Usually it is much larger in synthetic spinels than in natural spinels [59].

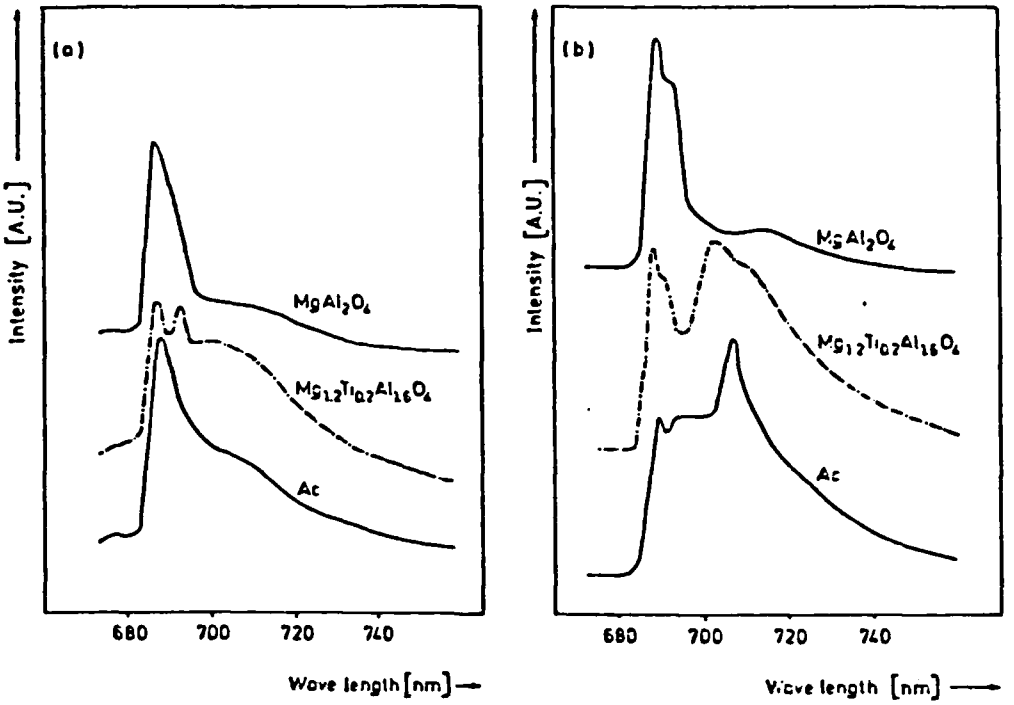

Figure 3a,b. Emission spectra of different samples under 590 nm laser excitation: a room temperature; b 4.4K [24].

In the spinel structure the Cr(III) impurities occupy octahedral cation positions [60]. Actually almost all Cr(III) complexes in solutions as well as in solid compounds are known to show coordination number N=6 with octahedral symmetry [38].

The spinels $MgAl_2O_4$ undergo inversion to some extent when heated between 750-900°C (and higher temperatures) without annealing [59]. Such inversion must occur to a considerable degree in the glass-ceramics Ac as evident from the appearance of additional lines due to $^2E \rightarrow {}^4A_2$ emissions resulting from the modified Cr(III) energy levels in the low symmetry characterizing cases of inverted spinel sites. This behaviour in crystals was thoroughly studied by Mikenda et al. [59-62].

The intrinsic $^2E \rightarrow {}^4A_2$ luminescence (R-line) has a lower intensity, as typical for strictly octahedral symmetry, than the

Cr(III) luminescence close to inverted sites [59]. This is not surprising, since the parity-forbidden transitions become partially allowed when the high symmetry is lowered. The R-line intensity increases when Cr(III) is excited at shorter wavelengths. A weak line at ~680 nm in the emission spectrum of glass-ceramics excited at 555 nm is the R-line [16]. This line is missing at 622 nm excitation. The next-most intensive line at 690-695 nm arises from Cr(III) in distorted octahedra CrO_6.

The so-called N lines [60-64] either originate in such distorted sites, or are due to interactions between two or more Cr(III) at relatively short mutual distances, also, implying anti-ferromagnetic coupling. The latter lines can usually be recognized by their increasing intensity as a function of higher Cr(III) concentration. In both cases [62,64] the lifetime of N line emission decreases systematically with their distance from R line emission on the regular octahedral sites, allowing differentiation by time-resolved spectroscopy having the advantage that transition to several components of $^4A_2$ from two or more Cr(III) have the same lifetime from a given excited state). Also, differing clusters can be distinguished by the positions of the $^4T_2$ maxima [61] of excitation spectra for N line emission.

The intensive but almost hidden line at 706 nm, the N_4-line [60-63] is due to the exchange-coupled Cr(III) ions (emission of Cr(III) pairs, which like the R line, changes its place only a little in the spectra of different spinels and many other crystals). The origin of this line from the Cr(III) pairs is deduced from lifetime measurements and time-resolved spectroscopy at low temperatures [11].

The gahnite glass-ceramics samples are prepared from a glass of starting composition 70.2 SiO_2, 15.0 Al_2O_3, 4.4 ZnO, 7.1 Li_2O, 1.5 TiO_2, 1.5 ZrO_2, 0.3 As_2O_3 mole% as described in reference 8. The specific glasses are doped by Cr(III) at a concentration of 1.1×10^{19} ions/cm^3.

The powdered crystalline samples of Cr(III) doped $ZnAl_2O_4$ gahnite were prepared for comparison from stoichiometric ratios of $Zn(NO_3)_3$ and $Al(NO_3)_3.9H_2O$ precipitated by aqueous ammonia, and the

mixed hydroxides calcined. The lattice constant a of the crystalline $ZnAl_2O_4$ was found by X-rays to be 8.085 Å.

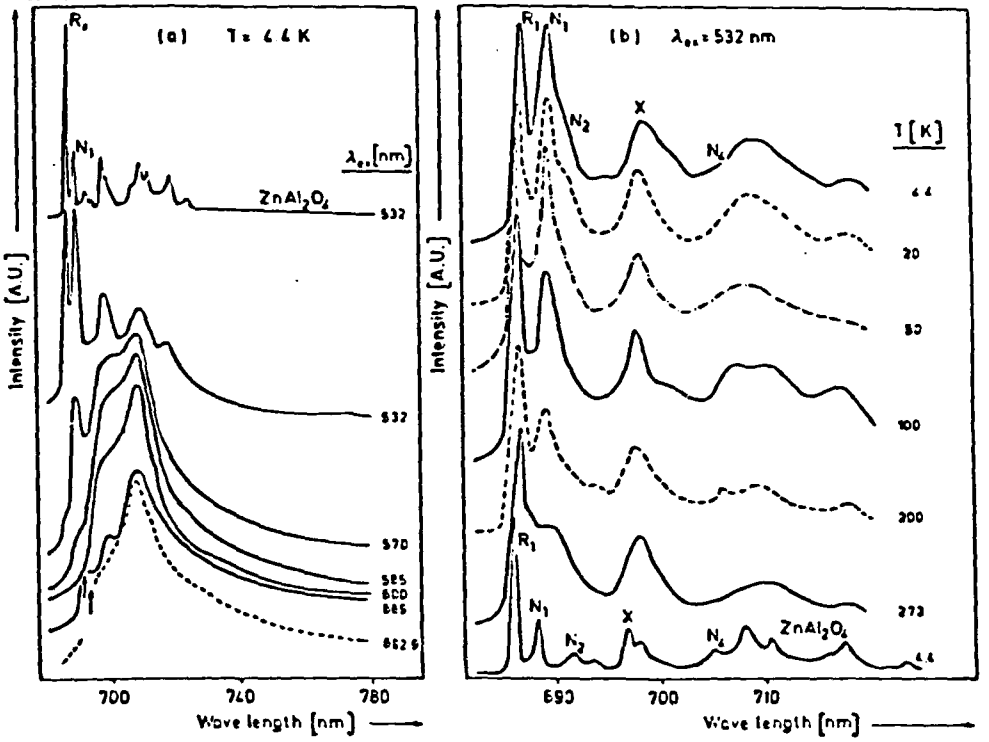

Figure 4. Comparison of the emission spectra of Cr(III) in $ZnAl_2O_4$ at λ_{ex}=532nm and temperature 4.4 with Cr(III) in gahnite glass-ceramics. a at various excitation wavelengths and temperature 4.4K; b at λ_{ex}=532nm and various temperatures [24].

Figures 4a and 4b present a comparison of the emission spectrum of Cr(III) in gahnite-like glass-ceramics at various excitation wavelengths at 4.4 K. We observe the R_1-line of Cr(III) at 686.2 nm both in $ZnAl_2O_4$ crystal and in glass-ceramics in contrast with $MgAl_2O_4$ synthetic crystal and in glass-ceramics where no such line appears [15]. The appearance of these lines is an evidence of Cr(III) in almost octahedral symmetry with no adjacent inverted site by analogy with the work of Mikenda et al. [60-62]. The N_1 (688.6 nm) line seen clearly both in the crystal and in glass-ceramics is actually ascribed to distorted Cr(III) sites. N_2 (692.3 nm) has much lower intensity than N_1 and is seen clearly in the crystal but is obscured in the

glass-ceramics. X (~697.0) is of comparable intensity with the N_1 line in the crystal and lower than the N_1 line in glass-ceramics. It has

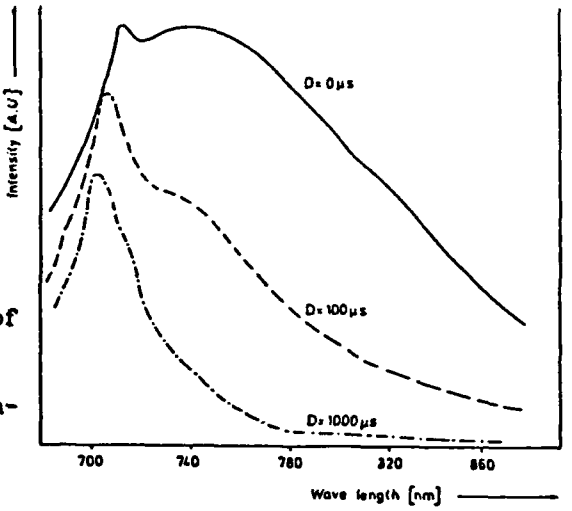

Figure 5. Time-resolved spectra of spinel-type glass-ceramics Ac excited at 680 nm at room temperature. The gate width is 100µs, D is the time delay [24].

been shown by Mikenda to decrease with the concentration of Cr(III) ions [60-62]. Therefore it has to be ascribed to singly perturbed ions. N_4 group of lines (705.0 to 715.0 nm) can be ascribed to distorted Cr(III) pairs. In the crystal three distinct lines can be seen and one broad band in the glass-ceramics as evident from Fig.4b. The intensity of these bands increases at lower temperature due to enhanced association of Cr(III) into pairs. The existence of such pairs was also detected by EPR measurements.

The excitation spectra of gahnite glass-ceramics due to $^4A_2 \rightarrow {}^4T_2$ broad-band absorption at 4.4 K are given in Fig.2 of Ref.12. The excitation peaks shift to lower energies in the order of selected emission wavelengths (given in parentheses):

R_1 line (682.2 nm)

N_1 line (688.6 nm)

X lines (701.2 nm)

$^4T_2 \rightarrow {}^4A_2$ (730 nm; maxima in excitation spectrum at 590 and 620 nm) same broad band (790 nm; maximum in excitation at 630 nm) which is consistent with the fact that the more regular Cr(III) sites show higher, and the pairs somewhat lower, field strengths.

Figure 5 shows several time-resolved emission spectra at 4.4 K under 570 nm excitation of spinel glass-ceramics. The R-line has the longest time-constant, the pairs exhibit the shortest time-constant as expected, while the perturbed ions are the intermediate case.

Immediately after excitation we see a broad band emission peaking at around 740 nm due to the $^4T_2 \rightarrow {}^4A_2$ transition. After longer times this emission decreases and a long-lived emission from the metastable state $^2E \rightarrow {}^4A_2$ peaking around 700 nm is observed.

The ^2E emission can be further resolved when the emission spectra are studied at liquid helium temperature, when the R line peaking at 685 nm is assigned to single Cr(III) ions and the one peaking at 705 nm to antiferromagnetically coupled pairs of Cr(III).

By comparing the emission spectra of Cr(III) in glass-ceramics with that of Cr(III) in single crystals one finds that the tendency to form pairs is greater in the glass-ceramics. In mixed crystals of spinel the appearance of Cr(III) pairs is again significant.

The variety of emission lines in the gahnite-like glass-ceramics and the possibility to ascribe these lines to various Cr(III) centres can be a useful tool in following the mechanisms of the nucleation of glass-ceramics doped by Cr(III). The high quantum efficiency of Cr(III) emission in glass-ceramics and the proximity of $^4T_2$ and ^2E levels in the distorted sites may have importance in designing tunable lasers.

7. TIME-RESOLVED SPECTROSCOPY OF Cr(III) IN MULLITE TRANSPARENT GLASS-CERAMICS

The investigation of Cr(III) in mullite glass-ceramics has been quite extensive [13,16,18,20,21].

The importance of these materials for luminescent solar concentrators and tunable lasers has been stressed [9,38]. The significant feature of Cr(III) in glass-ceramics is its high quantum efficiency of luminescence (0.91-1) at room temperature as opposed to only 0.07-0.19 in the parent glass [13].

The position of the $^4T_2$ state of Cr(III) in both media can be estimated from the absorption spectra [16]. There is a shift from 620

nm (16100 cm^{-1}) to 530-560 nm (18850-17850 cm^{-1}) in mullite glass-ceramics. The shift of the $^4T_2$ level to higher energies in glass-ceramics can be attributed to higher ligand fields in the latter. This fact can explain to some extent the lower relaxation rate of Cr(III) in mullite glass-ceramics since the crossing point between $^4T_2$ and the $^4A_2$ ground state will occur above the lowest vibrational levels of the $^4T_2$ state.

The decay curves for the glass-ceramics and glasses at ambient temperature and at 4.4 K deviated slightly from exponential behaviour over the wavelength range 680-720 nm in the vicinity of the ^2E level and deviated strongly in the 720-800 nm spectral range.

In glass-ceramics, the exponential part of the lifetime corresponds to about 9 ms at both 300 and 4.4 K in the range 680-750 nm. The longer lifetimes in glass-ceramics indicates, as expected, the higher fluorescence efficiency of Cr(III) in this medium. The emission intensity of ^2E has a quantum efficiency of about 0.9-1 both in glasses and glass-ceramics as inferred from the stability of the long component of the lifetime with temperature. However, in the case of glasses, a large part of the emission arises directly from the $^4T_2$ state as evident from the significant shortening of the lifetimes at longer emission wavelengths in glasses. This argument can be further pursued by inspection of the time-resolved spectra.

Fig.6 presents the time-resolved emission spectra of Cr(III) in glass at 4.4 K. Curve 1 in this figure is the integrated emission over a time interval of a few milliseconds. Curve 2, obtained after a delay of 0.1 μs, shows a strong emission from the $^4T_2$ state. This emission disappears, leaving only the long-lived emission from ^2E peaking at 698 nm.

The emission from the $^4T_2$ state is almost totally absent in glass-ceramics as evident from Fig.7. Only a very weak emission from this state is seen after a time delay of 0.1 μs taken a very high sensitivity; curve 1 taken after time integration of several milliseconds, curve 3 after a time delay of 0.2 ms, curve 4 after a delay of 1 ms and curve 5 after a delay of 10 ms when we can see an emission peaking at 698 nm. The same peak is also observed at room

temperature [13,16]. This is in contrast to the additional peaks at longer wavelengths in glass-ceramics based on spinels [15] and in

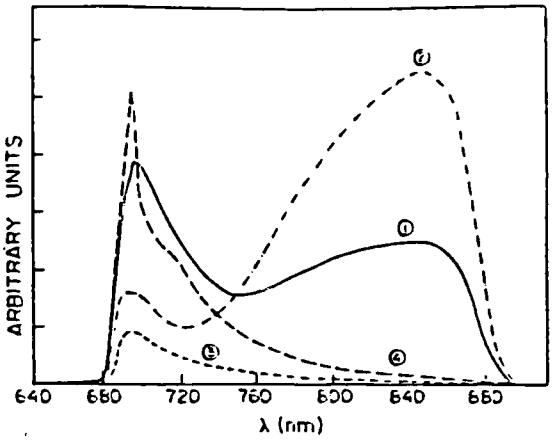

Figure 6. Emission spectrum of Cr(III)-doped parent glass under 532nm excitation at 4.4K. (1) Unresolved, time-integrated over several ms, (2) taken 0.1 μs after laser excitation, (3) taken 0.2ms after laser excitation, (4) taken 1ms after the laser pulse with sensitivity increased by a factor of 10 [18].

gahnite-type glass-ceramics [12] due to higher aggregates. No evidence for the existence of such aggregates is found in mullites. The crystalline phase of the mullite has a stoichiometric formula 2 Al_2O_3, SiO_2. Aluminium ions may be situated in both tetrahedral and octahedral sites in this structure [65].

Cr(III) enters the octahedral sites which are well isolated and do not allow formation of higher aggregates. This is the reason why Cr(III) can be incorporated at relatively high concentrations into the mullite phase without concentration quenching. Such a structure may be of great importance in designing highly luminescent materials.

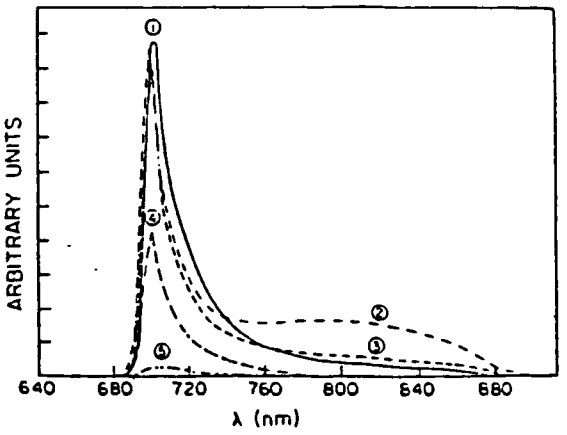

Figure 7. Emission spectrum of Cr(III) in mullite glass-ceramics under 532nm excitation at 4.4K. (1) Unresolved, time integrated over several ms, (2) taken 0.1 μs after laser excitation, (3) taken 0,2ms after laser excitation, (4) taken 1ms after laser excitation, (5) taken 10ns after laser excitation [18].

8. ENERGY TRANSFER FROM Cr(III) TO Nd(III) IN MULLITE GLASS-CERAMICS

Energy transfer between Cr(III) and Nd(III) in mullite glass-ceramics was studied by the dynamic method using laser excitation [19]. Comparison of the data with those of glasses shows that the energy transfer rate is higher in glasses, but the overall transfer efficiency is higher in glass-ceramics due to lower nonradiative relaxation of Cr(III) in the latter.

Fig.8 presents the absorption spectra of doped glass and glass-ceramics. Curve 1 presents the absorption spectrum of the precursor glass doped by 3 mole% of Nd(III) and 0.1 mole% of Cr(III). The absorption bands, in addition to the bands due to Nd(III), consist of two bands peaking at about 650 nm and about 450 nm which are due to Cr(III) ions situated in a low crystalline field [24]. Curve 2 presents the absorption spectrum of the precursor glass doped by 3 mole% of Nd(III) without addition of Cr(III), and curve 3 presents the absorption spectrum of glass-ceramics doped by 3 mole% Nd(III) and 0.1 mole% Cr(III).

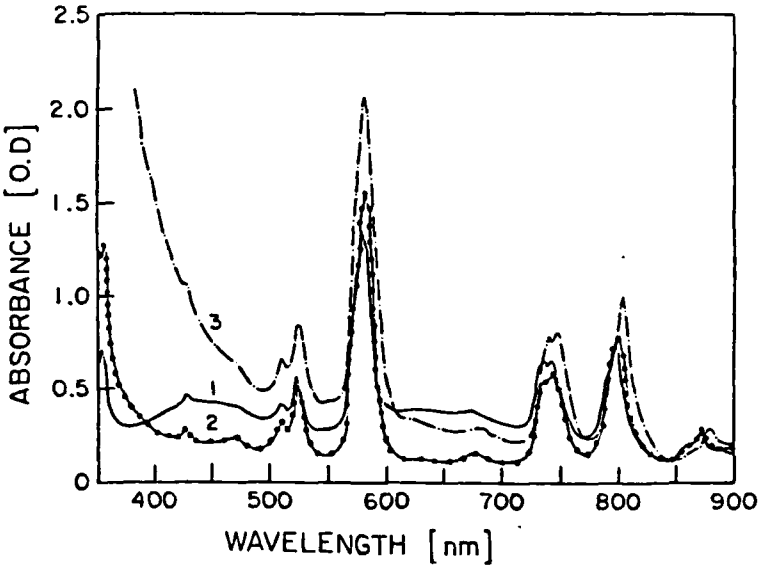

Figure 8. Absorption spectra: Curve 1; 3 mole% Nd(III), 0.1 mole% Cr(III) in precursor glass. Curve 2; 3 mole% Nd(III) in precursor glass. Curve 3; 3 mole% Nd(III), 0.1 mole% Cr(III) in mullite glass-ceramics [19].

The apparent absorption at shorter wavelengths in the glass-ceramics is due to Rayleigh scattering as confirmed by total polarization of the scattered light at 350 nm.

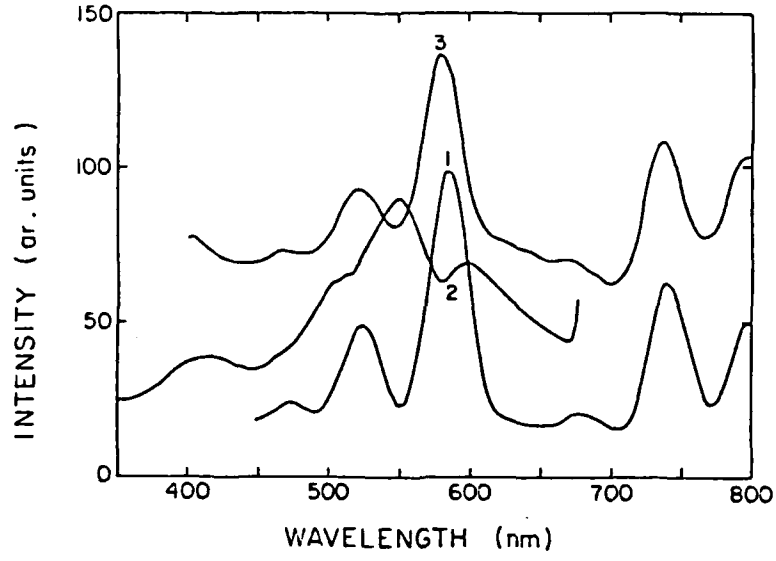

Figure 9. Excitation spectra: Curve 1; 3 mole% Nd(III) in mullite glass-ceramics detected at 880nm. Curve 2; 3 mole% Nd(III), 0.1 mole% Cr(III) in mullite glass-ceramics detected at 695nm. Curve 3; 3 mole% Nd(III), 0.1 mole% Cr(III) in glass-ceramics detected at 880nm [19].

Excitation spectra of the glass-ceramics are shown in Fig.9. Those spectra are vertically shifted for better visualization and are scaled to a similar height. Here curve 1 represents the excitation spectrum of glass-ceramics doped by 3 mole% Nd(III) without Cr(III) detected at 880 nm which corresponds to the transition $^4F_{3/2}$ --> $^4I_{9/2}$ of Nd(III). Curve 2 presents the excitation spectrum of mullite doped by 3 mole% of Nd(III) and 0.1 mole% of Cr(III) and detected at 695 nm, corresponding to two thermally equilibrated states $^2E_2$ and $^4T_2$ to the ground state $^4A_2$ of Cr(III) ions in mullite [16]. The dip at about 580 nm observed in this spectrum is due to absorption by the strong transition $^4I_{9/2}$ --> $^2G_{7/2}$ of Nd(III). In other respects this excitation spectrum is similar to the excitation spectrum of 0.1 mole% Cr(III) in mullite glass-ceramics without Nd(III). Curve 3 presents the excitation spectrum of the same glass-ceramics but detected at 880

nm, the emission band of Nd(III). Substantial broadening and a change in relative intensities of the excitation bands are noted. These can be due to energy transfer from Cr(III) to Nd(III) but also to some contribution of the emission of Cr(III) at the detection wavelength.

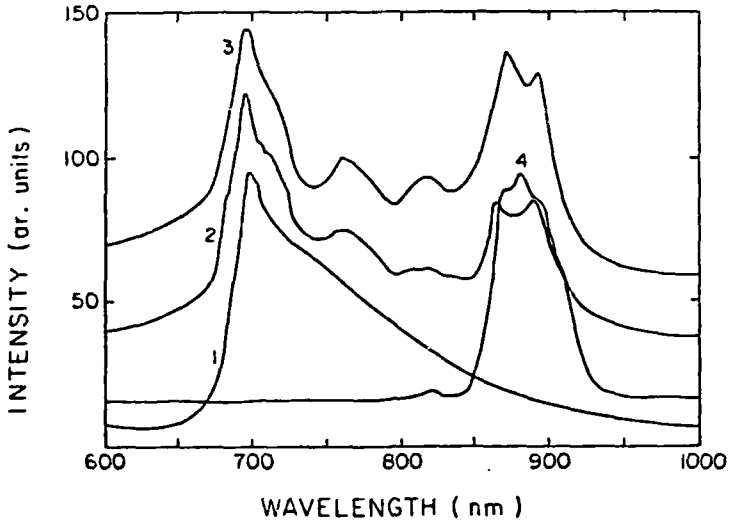

Figure 10. Emission spectra: Curve 1; 0.1 mole% Cr(III) excited at 550nm. Curve 2; 1 mole% Nd(III), 0.1 Cr(III) excited at 550nm. Curve 3; 3 mole% Nd(III), 0.1 mole% excited at 550nm. Curve 4; 3 mole% Nd(III excited at 550nm. All samples in mullite glass-ceramics [19].

Fig.10 presents the emission spectra of Nd(III) and Cr(III) in mullite glass-ceramics excited at 550 nm and vertically shifted for better visualisation. Curve 1 presents the emission spectrum of mullite glass-ceramics doped by 0.1 mole% of Cr(III). This is the characteristic emission band of the narrow $^2E_2$ linked via thermal equilibrium with the wide (and short lived) $^4T_2$ state which emit together to the ground state $^4A_2$. Curves 2 and 3 present the emission spectra of mullite glass-ceramics doped by 0.1 mole% of Cr(III) and co-doped by 1 mole% and 3 mole% of Nd(III) respectively. These curves are similar to curve 1 and the dips at about 750 and 800 nm are due to absorption by the strong absorption bands of Nd(III) (compare with Fig.8). The strong emission band at 820-920 nm is due to the transition $^4F_{3/2}$ --> $^4I_{9/2}$ of Nd(III). Curve 4 presents the emission

Table II: Lifetimes of Cr(III) and energy transfer parameters in mullite glass-ceramics codoped by Nd(III).

	Nd(III)	Cr(III)	Lifetime [μs]		Energy transfer yield [%]		Energy transfer rate $s^{-1}*10^{-3}$		reference
sample	mole%	mole%	τ_1	τ_2	1	2	k_1	k_2	
LLP	0	0.15	19.3	-*	-	-	-	-	66
LLP	3.08	0.15	4.1	-*	79	-	~192	-	66
g	0	0.1	6	7	-	-	-	-	16
g	3	0.1	3.6	5	42	29	~110	~57	19
gc	0	0.1	208	600	-	-	-	-	19
gc	1	0.1	60	136	71	35	~12	~2.5	19
gc	3	0.1	19	52	91	71	~48	~15	19

g - glass, gc - glass-ceramics, LLP - lithium-lanthanum phosphate, * - integrated lifetime.

spectrum of 3 mole% of Nd(III) in mullite glass-ceramics without Cr(III), excited at 550 nm. The emission range and consequently the tunability of the doubly doped glass-ceramics is wider than in glass-ceramics doped by Cr(III) only. This fact is of importance in designing tunable lasers. The decrease of lifetime of Cr(III) in the presence of Nd(III) indicates nonradiative energy transfer (radiative energy transfer is also observed as seen in Fig.10). The average energy transfer yields, η_1, corresponding to τ_1, and η_2, corresponding to τ_2, are calculated from these numbers according to formula;

$$\eta_i = 1 - \tau_i/\tau_o \qquad (1)$$

And energy transfer rate, k_{da};

$$k_{da} = 1/\tau_i - 1/\tau_o \qquad (2)$$

where τ_o is the lifetime of Cr(III) in mullite without addition of Nd(III). Table II summarizes the results. It should be noted that more than 90% of energy is transferred to Nd(III) within 20-30 μsec.

The third entry in Table II is the result of a previous work done on singly doped precursor glass. Lifetime of Cr(III) in this sample was compared with the lifetime of Cr(III) in the sample codoped by 3 mole% of Nd(III) (fourth entry). First and second entries are taken for comparison from the work on energy transfer from Cr(III) to Nd(III) in lithium-lanthanum phosphate glass. In glasses the energy transfer rates are much higher than in glass-ceramics, however the energy transfer yields are higher in the latter. This is rationalized by the higher radiative transition probability of Cr(III) in glass than in glass-ceramics, from which we see that the coupling between Cr(III) and Nd(III) in glass is stronger than in glass-ceramics. The higher integrated efficiency of transfer in the glass-ceramics on the other hand arises from longer lifetimes at which the process occurs.

Lifetimes of Nd(III) in these samples were found to be insensitive to the energy transfer process and are 200±10 μsec and 280±10 μsec for 3 mole% and 1 mole% of Nd(III) respectively, not different, within experimental error, from the lifetimes of Nd(III) in mullite without Cr(III). This is expected since the energy transfer takes place on a short times scale and the amount of energy transferred (per ion of Nd(III)) is small due to the small absorption of Cr(III) in mullite glass-ceramics.

A very recent study of energy transfer in these materials at low temperature [67] has revealed that the efficiency of energy transfer between Cr(III) and Nd(III) is much lower than at room temperature.

In summary, Cr(III) in glass-ceramics, because of its high efficiency and workability of materials, is promising material for tunable lasers and luminescent solar concentrators. The tunability range at room temperature may be extended by codoping the materials

with Nd(III) and utilizing the energy transfer between Cr(II) and Nd(III).

REFERENCES

1. Reisfeld, R. and Jørgensen, C.K., Structure and Bonding, 49 1 (1982)
2. Kisilev, A. and Reisfeld, R., Solar Energy, 33 163 (1984).
3. Avanesov, A.G., Voronko, Yu K., Denker, B.I., Kut'enkov, A.A. Maksimova, G.V. Osiko, V.V., Sidorova, E.I., Timofeev, Yu P. and Scherbakov, I.A., Sov. J. Quantum Electron., 9 1323 (1979).
4. Andrews, L.J., Lempicki, A. and McCollum, B.C., Chem. Phys. Lett., 74 404 (1980).
5. Andrews, L.J., Lempicki, A. and McCollum, B.C., J. Chem. Phys., 74 5526 (1981).
6. Kenyon, P.T., Andrews, L.J., McCollum, B.C. and Lempicki, A., IEEE J. Quantum Electron., QE-18 1189 (1982).
7. Kisilev, A., Reisfeld, R., Greenberg, E., Buch, A. and Ish-Shalom, M., Chem. Phys. Lett., 105 405 (1984).
8. Reisfeld, R., Kisilev, A., Greenberg, E., Buch, A. and Ish-Shalom, M., Chem. Phys. Lett., 104 153 (1984).
9. Reisfeld, R., Materials Science and Engineering, 71 375 (1985).
10. Buch, A., Ish-Shalom, M., Reisfeld, R., Kisilev, A. and Greenberg, E., Materials Science and Engineering, 71 383 (1985).
11. Bouderbala, M., Boulon, G., Reisfeld, R., Buch, A., Ish-Shalom, M. and Lejus, A.-M., Chem. Phys. Lett., 121 535 (1985).
12. Poncon, V., Bouderbala, M., Boulon, G., Lejus, A.-M., Reisfeld, R., Buch, A. and Ish-Shalom, M., Chem. Phys. Lett., 130 444 (1986).
13. Reisfeld, R., Kisilev, A., Buch, A. and Ish-Shalom, M., Chem. Phys. Lett., 129 446 (1986).
14. Kisilev, A., Reisfeld, R., Buch, A. and Ish-Shalom, M., Chem. Phys. Lett., 129 450 (1986).
15. Bouderbala, M., Boulon, G., Lejus, A.-M., Kisilev, A., Reisfeld, R., Buch, A. and Ish-Shalom, M., Chem. Phys. Lett., 130 438

(1986).

16. Reisfeld, R., Kisilev, A., Buch, A. and Ish-Shalom, M., J. Non-Cryst. Solids, **91** 333 (1987).
17. Poncon, V., Kalisky, Y., Boulon, G. and Reisfeld, R., Chem. Phys. Lett., **133** 363 (1987).
18. Kalisky, Y., Poncon, V., Boulon, G., Reisfeld, R., Buch, A. and Ish-Shalom, M., Chem. Phys. Lett., **136** 368 (1987).
19. Reisfeld, R. Eyal. M., Buch, A. and Ish-Shalom, M., Chem. Phys. Lett., **147** 148 (1988).
20. Andrews, L.J., Beall, G.H. and Lempicki, A., J. Luminescence, **36** 65 (1986).
21. Wojtowicz, A.J. and Lempicki, A., J. Luminescence, **39** 189 (1988).
22. Bergin, F.J., Donegan, J.F., Glynn, T.J. and Imbusch, G.F., J. Luminescence, **34** 307 (1986); **36** 231 (1987).
23. Bruce, A., Capobianco, J.A., Cormier, G., Krashkevich, D. and Simkin, D.J., J. de Physique, Colloque C7, Supplement au No.12, **48** C7-459 (1987).
24. Reisfeld, R. and Jørgensen, C.J., Structure and Bonding, **69** 63 (1988).
25. Reisfeld, R. and Jørgensen, C.K., Cr(III) broad-band quartet-quartet luminescence in glass-ceramics with higher yield than in complexes. E.L. King, D.H. Busch and R.E. Sievers, (eds.). Abstracts of 23rd Intl. Conf. Coordination Chemistry, Boulder CO 1984, p.162.
26. Jørgensen, C.K., **Oxidation Numbers and Oxidation States**, Springer-Verlag, Berlin-Heidelberg-New York 1969.
27. Sugano, S., Tanabe, Y. and Kamimura, H., **Multiplets of Transition Metal Ions in Crystals**, Academic Press, New York, 1970.
28. Reisfeld, R. and Kisilev, A., Chem. Phys. Lett., **115** 457 (1985).
29. Van Die, A., Leenaers, A.C.H.I., Blasse, G. and Van der Weg, W.F., J. Non-Cryst. Solids, **99** 32 (1988).
30. Jørgensen, C.K., **Absorption Spectra and Chemical Bonding in Complexes**, Pergamon, Oxford, 1962, 2nd ed. 1964.
31. Jørgensen, C.K., Adv. Chem. Phys., **5** (1963) 33.
32. Jørgensen, C.K., **Modern Aspects of Ligand Field Theory**, North-

Holland, Amsterdam, 1971.

33. McClure, D.S., Solid State Phys., 9 399 (1963).
34. McClure, D.S., J. Chem. Phys., 36 2759 (1962); 38 2289 (1963).
35. Reinen, D., Structure and Bonding, 6 30 (1969).
36. Reisfeld, R., Eyal, M. and Jørgensen, C.K., Chimia, 41 117 (1987).
37. Reisfeld, R., Eyal, M., Guenther, A.H. and Bendow, B., Chimia, 40 403 (1986).
38. Reisfeld, R., Potential uses of Cr(III) doped transparent glass-ceramics in luminescent solar concentrators. Report Series Swedish Academy of Engineering Sciences in Finland (Helsinki) 40, part I (Proc. Advanced Summer School on the Electronic Structure of New Materials, Loviisa, August 1984) pp. 7-24, Helsinki 1985.
39. Jørgensen, C.K., Faucher, M. and Garcia, D., Chem. Phys. Lett., 128 250 (1986).
40. Reisfeld, R. and Jørgensen, C.K., Handbook on the Physics and Chemistry of Rare Earths (eds. Gschneidner, K.A., Eyring, L.) 9 chapter 58, pp. 1-90, North-Holland, Amsterdam 1987.
41. Reisfeld, R. and Jørgensen, C.K., **Lasers and Excited States of Rare Earths**, Springer-Verlag, Berlin-Heidelberg-New York 1977.
42. Jørgensen, C.K. and Reisfeld, R., Structure and Bonding, 50 121 (1982).
43. Jørgensen, C.J., Acta Chem. Scand., 8 1495 (1954).
44. Schaffer, C.E., J. Inorg. Nucl. Chem., 8 149 (1958).
45. Porter, G.B. and Schlafer, H.L., Z. Physik. Chem., 37 109 (1963).
46. Ferguson, J., Guggenheim, H.J. and Wood, D.L., J. Chem. Phys., 54 504 (1971).
47. Jørgensen, C.J., Acta Chem. Scand., 9 1362 (1955); 10 887 (1956).
48. Reedijk, J., van Leeuwen, P.W.N.M. and Groeneveld, W.L., Rec. trav. chim. Pay-Bas 87 129 (1968).
49. Griffith, J.S., **The Theory of Transition-metal Ions**, Cambridge University Press 1961.
50. Condon, E.U. and Shortley, G.H., **Theory of Atomic Spectra**, Cambridge University Press 1953.
51. Jørgensen, C.K. and Schwochau, K., Z. Naturforsch., 20a 65 (1965).
52. Schaffer, C.E. and Jørgensen, C.K., J. Inorg. Nucl. Chem., 8 143

(1958).

53. Jørgensen, C.K., Acta Chem. Scand., 10 500 (1956); 11 151 (1957).
54. Schroder, K.A., J. Chem. Phys. 37 2553 (1962).
55. Boulon, G., Materials Chemistry and Physics, 16 301 (1987).
56. Wang, M.L., Stevens, R. and Knott, P., Glass Technology, 23 238 (1982).
57. Durville, F., Champagnon, B., Duval, E., Boulon, G., Gaume, F., Wright, A.F. and Fitch, A.N., Phys. Chem. Glasses 25 126 (1984).
58. Durville, F., Champagnon, B., Duval, E. and Boulon, G., Phys. Chem. Solids, 46 701 (1985).
59. Derkosch, J., Mikenda, W. and Preisinger, A., Spectrochim. Acta, 32A 1759 (1976).
60. Mikenda, W. and Preisinger, A., J. Luminescence, 26 53 and 67 (1981).
61. Mikenda, W., J. Luminescence, 26 85 (1981).
62. Derkosch, J. and Mikenda, W., J. Luminescence, 28 431 (1983).
63. Imbusch, G.F. in **Energy Transfer Processes in Condensed Matter** (ed. DiBartolo, B.) 114 47 (1984), Plenum Press, New York.
64. Gorkom, G.G.P. van, Henning, J.C.M. and Stapele, R.P. van, Phys. Rev., B8 955 (1973).
65. Sadanaga, R., Tokonami, M. and Takeuchi, Y., Acta Cryst., 15 65 (1962).
66. Reisfeld, R., Inorg. Chim. Acta, 140 345 (1987).
67. Kalisky, Y., Boulon, G. and Reisfeld, R., unpublished results.

From our experimental data presented in the text it is possible to calculate the stimulated emisssion cross-section and laser threshold for Cr(III) doped glass-ceramics. An example of such calculations for Cr(III) in mullite glass-ceramics is presented below.

1. STIMULATED CROSS-SECTION

For this purpose we use the model for a phonon terminated three-level laser developed by McCumber [1]. This model allows the calculation of the stimulated cross-section for emission by use of experimental parameters such as lifetime of the lasing level, quantum yield and corrected emission spectrum. In an isotropic medium we may write,

$$\sigma_e(\tilde{\nu}) = \lambda^2 \cdot f(\tilde{\nu}) \qquad (1)$$

where λ is the pumping wavelength. The function is in units of photons/sec^{-1} per unit frequency interval.

On the other hand,

$$\frac{\eta}{\tau} = 8\pi \cdot c \cdot \int f(\tilde{\nu}) d\tilde{\nu} \qquad (2)$$

where η is the quantum yield and τ is the lifetime of the lasing level. The factor 8π arises from integration over the solid angle and the two polarization orientations and the speed of light, c, is introduced to convert the frequency units from sec^{-1} to cm^{-1}.

This integrated intensity is related to the integral of the experimental corrected emission spectrum by a relation,

$$\gamma \cdot \int f(\tilde{\nu}) d\tilde{\nu} = \int F(\tilde{\nu}) d\tilde{\nu} \qquad (3)$$

where γ is a proportionality factor and $\tilde{\nu}$ runs over cm^{-1}.

Taking the average value of quantum yield for mullite as 0.7 and the first-fold lifetime τ_1 = 208 microseconds [2] we obtain from eq.2,

$$\frac{\eta}{\tau} = 3.36 \cdot 10^{3}/\text{sec} \quad \text{and thus} \quad \int f(\nu)d\nu = 4.46 \cdot 10^{-9}/\text{cm}$$

Integration of the corrected emission spectrum, excited at 550 nm gives 1.332×10^{5}/cm, which allows the determination of the proportionality factor, γ, using eq.3 as being equal to 0.269×10^{14}.

At 700 nm (14285.7/cm) the experimental corrected emission intensity is 60 units, hence, using the proportionality factor we get,

$$f(\nu) = 2.23 \cdot 10^{-12}$$

Substituting this value into formula 1 we obtain, at pumping wavelength of 550 nm,

$$\sigma_e = 0.675 \text{ pm}^2$$

This cross-section can be compared to the cross-section obtained for Cr(III) in gallium scandium gadolinium garnet (GSGG) at 756 nm, which is 0.7 pm^2 [3], and for alexandrite at 750 nm, 0.76 pm^2 [4].

2. THRESHOLD POWER FOR LASER ACTION

The formula for calculating the laser threshold power for longitudinal pumping (in units of mW/cm^2) is [3],

$$P_t = N_t \cdot h\nu \cdot V/\tau \qquad (4)$$

where $h\nu$ is the photon energy of the pumping light, V is the rod volume excited by the dye laser and $N_t = N_2 - N_1$, the threshold inversion density, where N_2 and N_1 are the excited and the ground state densities respectively, is defined by,

$$N_t = (L+T)/(2 \cdot \sigma_e \cdot l) \qquad (5)$$

Let's choose the rod length as 1 cm, and a doping concentration of 0.1 w.p. of Cr_2O_3 (1.8×10^{19} /cm^3). The laser is pumped longitudinally by a CW dye laser at 550 nm. These conditions are common throughout the relevant literature. Scattering losses of the glass ceramics are of the order of 1%/cm [5] and mirrors transmittance, T, of the order of 2%. Taking into account possible absorption of the excited state [6] we intentionally overestimate the total cavity losses and set L = 10%.

Substituting these values and the value of stimulated cross-section into eq.5 we obtain $N_t = 0.74 \times 10^{19}$ /cc.

The threshold absorbed power is then calculated from formula 4 by using a typical value of pumping beam radius of 25 micrometer for which V equals 1.96×10^{-5} cc and obtain P_t=252 mW/cm^2.

This value scales linearly with the total cavity losses, hence for L+T = 0.05, which is a value commonly reported in literature, the threshold power should be halved to the value of 126 mW/cm^2.

Absorption cross-section of Cr(III) in mullite glass-ceramics at 550 nm is about 4 pm^2 [2]. At the density of 1.8×10^{19} /cc it results in absorption of 81% of the pumping beam. Hence the incident threshold power is, $P_i = P_t/0.81$=311.1 mW/cm^2.

REFERENCES

1. D.E. McCumber, Phys.Rev., 134A (1964) 299; 136A (1964) 954.
2. R. Reisfeld, M. Eyal, A. Buch and M. Ish-Shalom, Chem. Phys. Lett., 147 (1988) 148.
3. B. Struve and G. Huber, J. Appl. Phys., 57 (1985) 45.
4. J.C. Walling, H.P. Jensen, R.C. Morris, E.W. O'Dell and O.G. Petersen, Opt. Lett., 4 (1979) 182.
5. L.J. Andrews, G.H. Beall, A. Lempicki, J. Lumin., 36 (1986) 65.
6. W. Seelert and E. Strauss, Private communication.

4697-MS

TRANSPARENT GLASS CERAMICS DOPED BY CHROMIUM(III) AND CHROMIUM(III) AND NEODYMIUM(III) AS NEW MATERIALS FOR LASERS AND LUMINESCENT SOLAR CONCENTRATORS

Research supported by U.S. Army
under contract No. DAJA 45-85-C-0051

Intermediate Report
1.1.88 - 30.6.88

Submitted by

Professor Renata Reisfeld
Department of Inorganic and Analytical Chemistry
The Hebrew University of Jerusalem
Jerusalem 91904 Israel

to

European Office of the U.S. Army
223/231 Old Marylebone Rd.

and

Army Materials and Mechanics
Research Center, Watertown,

This work was performed together with Marek Eyak, Alla Buch and Moshe Ish-Shalom.

ENERGY TRANSFER FROM CHROMIUM(III) TO NEODYMIUM(III) IN MULLITE GLASS-CERAMICS *

Renata REISFELD [1], Marek EYAL
Department of Inorganic and Analytical Chemistry, The Hebrew University, Jerusalem 91904, Israel

Alla BUCH and Moshe ISH-SHALOM
Israel Ceramics and Silicate Institute, Technion City, Haifa 32000, Israel

Received 17 March 1988

Energy transfer between Cr(III) and Nd(III) in mullite glass-ceramics was studied by a dynamic method using laser excitation. Comparison of the data with those of glasses shows that the energy transfer rate is higher in glasses, but the overall transfer efficiency is higher in glass-ceramics due to the lower rate of non-radiative relaxation of Cr(III) in the latter.

1. Introduction

Tunable lasers based on organic dyes are well known and their applications in various branches of physics and chemistry are well established. Because of degradation of the dyes under severe external conditions there is a need to replace the organic molecules by inorganic ions incorporated in a stable inorganic matrix which have the optical properties and the tunability range of the organic dyes but do not suffer the disadvantage of degradation. One such material is single-crystal alexandrite doped by trivalent chromium. We have shown previously [1] that the spectroscopic properties of Cr(III) in several singly doped glass-ceramics are comparable to those of alexandrite and the preparation is much easier and more economical. Preparation procedures [2], steady-state EPR spectroscopy [3] and time-resolved spectroscopy [4] in mullite glass-ceramics doped by Cr(III) were studied by us prior to this work. In contrast to other glass-ceramics where Ti(IV) is used as a nucleating agent, the nucleating agent in mullite is Cr(III) itself [5]. Energy transfer between Nd(III) and Cr(III) can increase the tunability range of Nd(III) lasers and the efficiency of solar collectors [6,7]; therefore energy transfer between these two ions was studied here in mullite glass-ceramics. The results are compared with those for precursor glass of the same composition (prior to thermal treatment) and also with doubly doped lithium lanthanum phosphate glass studied by us recently [7].

2. Experimental procedure

The starting composition of the precursor glasses (in mol%) was as follows: 45 SiO_2, 20 B_2O_3, 25 Al_2O_3, 10 K_2O, x Nd_2O_3 and y Cr_2O_3 where x and y are specified in table 1. The glasses were prepared by melting the precursor mixture in alumina crucibles in an electric furnace heated to 1600°C, pouring into a steel mould and placing in a furnace preheated to 650°C for annealing. The furnace was immediately turned off and the glasses were allowed to cool at the cooling rate of the furnace. For the preparation of mullite glass-ceramics the glasses were heat-treated in two steps: Samples containing 3 mol% of Nd(III) were first heated at 700°C for 2 h, then at 750°C for 3 h and finally cooled at the cooling rate of the furnace; samples containing 1 mol% of Nd(III) were heated at 750°C for 10 h, at 860°C for 2 h and then cooled at the cooling rate of the furnace. The cooled

* Supported by US Army Contract DAJA 45-85-c-0051.
[1] Enrique Berman Professor of Solar Energy.

0 009-2614/88/$ 03.50 © Elsevier Science Publishers B.V.
(North-Holland Physics Publishing Division)

Table 1
Preparation conditions for mullite glass-ceramics doped by Nd(III) and/or Cr(III)

Sample number	Nd(III) (mol%)	Cr(III) (mol%)	Thermal treatment		Color
			T_1 (°C/h)	T_2 (°C/h)	
1	1	0.0	-	-	pale lilac
2	3	0.0	-	-	lilac
3	1	0.1	-	-	green
4	3	0.1	-	-	lilac-green
5	1	0.0	750/10	860/2	very pale lilac
6	3	0.0	700/2	750/3	lilac
7	1	0.1	750/10	860/2	pale grey-lilac
8	3	0.1	700/2	750/3	greyish lilac
9	0	0.1	750/2	800/4	grey

material was cut and polished. Mole percents of the dopants, thermal treatments and color of the glasses/glass-ceramics are summarized in table 1, where entries 1 to 4 refer to doped precursor glasses without thermal treatment.

Absorption spectra of the doped samples were measured on a Lambda-5 Perkin–Elmer double beam spectrophotometer against air since different sample sizes precluded the use of a single glass as a reference for all. Emission and excitation spectra were measured on a home-made spectrofluorimeter consisting of an Oriel 150 W xenon lamp source, an Oriel excitation monochromator, a Spex-1704 analyzing monochromator and a Peltier-cooled Hamamatsu 7102 photomultiplier coupled to a PAR-128 lock-in amplifier. All measurements were performed at room temperature. Polarization measurements were performed on a Jasco-770 spectrofluorimeter. The samples were excited by light polarized parallel to the plane of incidence. The emitted light was analyzed by means of a Polaroid polarizer and the intensities of the parallel and the perpendicular components of the emitted light were compared.

Lifetimes were measured using a tunable dye laser, Molectron-DL200 pumped by a Molectron UV-4 pulsed nitrogen laser at a repetition rate of 10 Hz and pulse duration of about 10 ns. For excitation of Cr(III) at 530 nm a coumarin dye, and for excitation of Nd(III) at 595 nm a rhodamine 6G dye were used. The emitted light was passed through a monochromator and detected with a R928 Hamamatsu photomultiplier. The signals were then sampled by a Biomation 8100 digitizer (10 ns resolution) and averaged with a Nicolet 178 analyzer. The averaged decay curves were then recorded on a YEW recorder. For further analysis the recorded signals were fed into a PC where they were processed.

3. Results and discussion

Fig. 1 presents the absorption spectra of doped glass and glass-ceramics. Curve 1 presents the absorption spectrum of the precursor glass doped by 3 mol% Nd(III) and 0.1 mol% Cr(III). The absorption bands, in addition to the bands due to Nd(III), consists of two bands peaking at about 650 and 450 nm which are due to Cr(III) ions situated in a low crys-

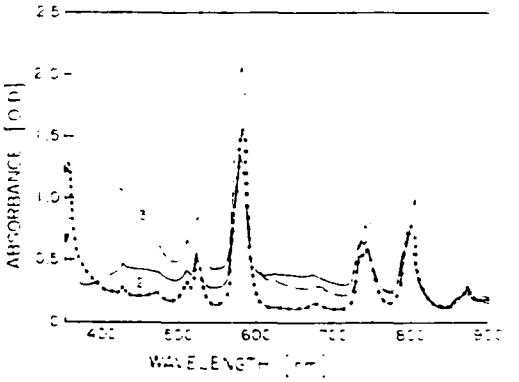

Fig. 1. Absorption spectra. Curve 1: 3 mol% Nd(III), 0.1 mol% Cr(III) in precursor glass. Curve 2: 3 mol% Nd(III) in precursor glass. Curve 3: 3 mol% Nd(III), 0.1 mol% Cr(III) in mullite glass-ceramics.

Table 2
Intensity parameters for Nd(III) in mullite glass-ceramics and in silica glass

Glass	Ref.	Ω_2 (pm^2)	Ω_4 (pm^2)	Ω_6 (pm^2)
silicate	[8]	4.4	3.0	2.6
mullite	this work	2.4	1.9	2.8
mullite + Cr	this work	2.3	2.0	3.2

talline field [1]. Curve 2 presents the absorption spectrum of the precursor glass doped by 3 mol% Nd(III) without addition of Cr(III), and curve 3 presents the absorption spectrum of glass-ceramics doped by 3 mol% Nd(III) and 0.1 mol% Cr(III).

The apparent absorption at shorter wavelengths in the glass-ceramics is due to Rayleigh scattering as confirmed by total polarization of the scattered light at 350 nm.

The absorption spectra of Nd(III) serve as a basis for a complete set of predictions of transition rates within the $4f^3$ configuration of Nd(III). The procedure is based on the theory of Judd and Ofelt and is described in detail elsewhere [8]. The intensity parameters Ω_i calculated for Nd(III) in the mullite glass-ceramics with and without Cr(III) are given in table 2 and compared with the corresponding value in a silicate glass (H(11) – 67 SiO_2, 18 BaO, 15 K_2O) [9].

Excitation spectra of the glass-ceramics are shown in fig. 2. These spectra are vertically shifted for better visualization and are scaled to a similar height. Here curve 1 represents the excitation spectrum of glass-ceramics doped by 3 mol% Nd(III) without Cr(III) detected at 880 nm which corresponds to the transition $^4F_{3/2} \rightarrow {}^4I_{9/2}$ of Nd(III). Curve 2 presents the excitation spectrum of mullite doped by 3 mol% Nd(III) and 0.1 mol% Cr(III) and detected at 695 nm, corresponding to transitions from thermally equilibrated states ^2E and $^4T_2$ to the ground state $^4A_2$ of Cr(III) ions in mullite [2]. The dip at about 580 nm observed in this spectrum is due to absorption by the strong transition $^4I_{9/2} \rightarrow {}^4G_{5/2}$ of Nd(III). In other respects this excitation spectrum is similar to the excitation spectrum of 0.1 mol% Cr(III) in mullite glass-ceramics without Nd(III). Curve 3 presents the excitation spectrum of the same glass-ceramics but detected at 880 nm, the emission band of Nd(III). Substantial broadening and a change in

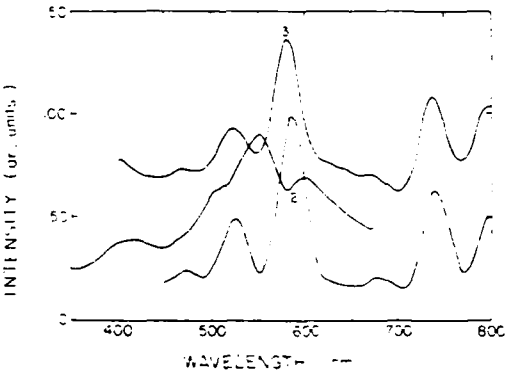

Fig. 2. Excitation spectra. Curve 1: 3 mol% Nd(III) in mullite glass-ceramics, detected at 880 nm. Curve 2: 3 mol% Nd(III), 0.1 mol% Cr(III) in mullite glass-ceramics, detected at 695 nm. Curve 3: 3 mol% Nd(III), 0.1 mol% Cr(III) in glass-ceramics, detected at 880 nm.

relative intensities of the excitation bands are noted. This may be due to energy transfer from Cr(III) to Nd(III) but also to a contribution from the emission of Cr(III) at the detection wavelength.

Fig. 3 presents the emission spectra of Nd(III) and Cr(III) in mullite glass-ceramics excited at 550 nm and vertically shifted for better visualisation. Curve 1 presents the emission spectrum of mullite glass-ceramics doped by 0.1 mol% of Cr(III). This is the characteristic emission band of the narrow ^2E state

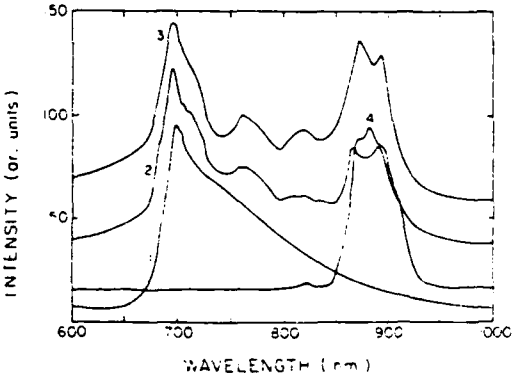

Fig. 3. Emission spectra. Curve 1: 0.1 mol% Cr(III) in mullite glass-ceramics, excited at 550 nm. Curve 2: 1 mol% Nd(III), 0.1 mol% Cr(III) in mullite glass-ceramics, excited at 550 nm. Curve 3: 3 mol% Nd(III), 0.1 mol% Cr(III) in mullite glass-ceramics, excited at 550 nm. Curve 4: 3 mol% Nd(III) in mullite glass-ceramics, excited at 550 nm.

linked via thermal equilibrium with the wide (and short-lived) $^4T_2$ state which emit together to the ground state $^4A_2$. Curves 2 and 3 present the emission spectra of mullite glass-ceramics doped by 0.1 mol% Cr(III) and co-doped by 1 and 3 mol% Nd(III), respectively. These curves are similar to curve 1 and the dips at about 750 and 800 nm are due to absorption by the strong absorption bands of Nd(III) (compare with fig. 1). The strong emission band at 820–920 nm is due to the transition $^4F_{3/2} \rightarrow {}^4I_{9/2}$ of Nd(III). Curve 4 presents the emission spectrum of 3 mol% of Nd(III) in mullite glass-ceramics without Cr(III), excited at 550 nm. The emission range *and consequently the tunability* of the doubly doped glass-ceramics is wider than in glass-ceramics doped by Cr(III) only. This fact is of importance in designing tunable lasers. The decrease in the lifetime of Cr(III) in the presence of Nd(III) indicates non-radiative energy transfer (radiative energy transfer is also observed as seen in fig. 3). In order to quantitatively measure the transfer efficiencies and transfer rates we first measured the anisotropy of emission of Cr(III) and found that the sample excited by polarized light at 530 nm emits light at 695 nm whose parallel/perpendicular components ratio is 3:1, equal to the theoretical ratio derived for randomly distributed emitting species without migration of energy. Thus having established that an excited Cr(III) ion can transfer energy only to its nearest neighbour Nd(III) ion, we excited the samples at 530 nm by a dye laser and the transient signals were detected at 695 nm, which is the wavelength of maximum emission of Cr(III) in mullite and at which Nd(III) does not emit. Due to high non-exponentiality of the decay curves we characterized the lifetimes τ_1 as the time required for the transient signal to decay to 1/e of its intensity at time 0 and τ_2 as half of the time for decay to $1/e^2$ of the initial intensity. In the case of an exponential decay these numbers are equal. The average energy transfer yields, η_1, corresponding to τ_1, and η_2, corresponding to τ_2, are calculated from these numbers according to

$$\eta_i = 1 - \tau_i/\tau_0 \qquad (1)$$

and the energy transfer rate, k_{da}, according to

$$k_{da} = 1/\tau_i - 1/\tau_0 \,, \qquad (2)$$

where τ_0 is the lifetime of Cr(III) in mullite without addition of Nd(III). Table 3 summarizes the results. It should be noted that more than 90% of the energy is transferred to Nd(III) within 20–30 μs.

The third entry in table 3 is the result of previous work on singly doped precursor glasses. The lifetime of Cr(III) in this sample was compared with the lifetimes of Cr(III) in the sample co-doped by 3 mol% Nd(III) (fourth entry). The first and second entries for comparison are taken from the work on energy transfer from Cr(III) to Nd(III) in lithium lanthanum phosphate glass. In glasses the energy transfer rates are much higher than in glass-ceramics; however the energy transfer yields are higher in the latter. This can be rationalized by the higher radiative transition probability of Cr(III) in glass than in

Table 3
Lifetimes of Cr(III) and energy transfer parameters in mullite glass-ceramics co-doped by Nd(III)

Sample [a]	Nd(III) (mol%)	Cr(III) (mol%)	Lifetime (μs)		Energy transfer				Ref.
			τ_1	τ_2	yield (%)		rate (1/ms)		
					η_1	η_2	k_1	k_2	
LLP	0	0.15	19.3	– [b]	–	–	–	–	[7]
LLP	3.08	0.15	4.1	– [b]	79	–	≈ 192	–	[7]
g	0	0.1	6	–	–	–	–	–	[2]
g	3	0.1	3.6	5	42	29	≈ 110	≈ 57	this work
gc	0	0.1	208	600	–	–	–	–	this work
gc	1	0.1	60	136	71	35	≈ 12	≈ 2.5	this work
gc	3	0.1	19	52	91	71	≈ 48	≈ 15	this work

[a] g, glass; gc, glass-ceramics. LLP, lithium lanthanum phosphate. [b] Integrated lifetime.

glass-ceramics, from which we see that the coupling between Cr(III) and Nd(III) in glass is stronger than in glass-ceramics. The higher integrated efficiency of transfer in the glass-ceramics on the other hand arises from the longer lifetime at which the process occurs.

Lifetimes of Nd(III) in these samples were found to be insensitive to the energy transfer process and are 200±10 and 280±10 μs for 3 and 1 mol% Nd(III) respectively, not different, within experimental error, from the lifetimes of Nd(III) in mullite without Cr(III). This is expected since the energy transfer takes place on a short timescale and the amount of energy transferred (per ion of Nd(III)) is small due to the small absorption of Cr(III) in mullite glass-ceramics.

4. Conclusions

Our study of mullite glass-ceramics doped by Cr(III) and Nd(III) indicates that the tunability range of such material is wider than in the singly doped glass-ceramics. Both non-radiative and radiative energy transfer have been observed in this material. The non-radiative energy transfer is more efficient in glass-ceramics than in precursor glass, though the energy-transfer rate is much slower. This indicates that the weaker coupling is more than compensated by the long lifetime of Cr(III) in the glass-ceramics, which leads to a higher overall energy-transfer yield.

References

[1] R. Reisfeld and C.K. Jørgensen, Struct. Bonding 69 (1988).
[2] R. Reisfeld, A. Kisilev, A. Buch and M. Ish-Shalom, J. Non-Cryst. Solids 91 (1987) 333.
[3] R. Reisfeld, A. Kisilev, A. Buch and M. Ish-Shalom, Chem. Phys. Letters 129 (1986) 446.
[4] Y. Kalisky, V. Poncon, G. Boulon, R. Reisfeld, A. Buch and M. Ish-Shalom, Chem. Phys. Letters 136 (1987) 368.
[5] G.H. Beal, J. Non-Cryst. Solids 73 (1985) 413.
[6] R. Reisfeld, Inorg. Chim. Acta 140 (1987) 345.
[7] R. Reisfeld and A. Kisilev, Chem. Phys. Letters 115 (1985) 457.
[8] R. Reisfeld and C.K. Jørgensen, Lasers and excited states of rare earths (Springer, Berlin, 1977).
[9] R.R. Jacobs and M.J. Weber, IEEE J. Quantum Electron. QE 10 (1974) 450.